Journal of Solid State Chemistry **168,** 597–607 (2002)
doi:10.1006/jssc.2002.9757

Synthesis and Electroconductive Properties of Radical Salts Derived from Tetrathiafulvalene Dimers

Masahiko Iyoda,*[,1] Kenji Hara,* Eiji Ogura,* Takahiro Takano,* Masashi Hasegawa,* Masato Yoshida,* Yoshiyuki Kuwatani,* Hiroyuki Nishikawa,* Koichi Kikuchi,* Isao Ikemoto,* and Takehiko Mori†

*Department of Chemistry, Graduate School of Science, Tokyo Metropolitan University, 1-1 Minami-ohsawa, Hachioji, Tokyo 192-0397, Japan; and †Department of Organic and Polymeric Materials, Tokyo Institute of Technology, O-okayama, Tokyo 152-8552, Japan

Received January 15, 2002; in revised form April 30, 2002; accepted May 13, 2002

Palladium(II)- or copper(II)-catalyzed homo-coupling reaction of either trimethylstannyltetrathiafulvalene or tetrathiafulvalenylzinc chloride produces symmetrical bitetrathiafulvalenes (bi-TTFs) in good yields, whereas palladium(0)-catalyzed cross-coupling reaction of tetrathiafulvalenylzinc chloride with 4-iodotetrathiafulvalenes leads to the corresponding unsymmetrically substituted bi-TTFs in moderate-to-high yields. The X-ray analysis of bi-TTF derivatives showed planar structures, and the cyclic voltammetry suggested that bi-TTFs have good donor ability comparable to that of BEDT-TTF. The symmetrical bi-TTFs formed the corresponding CT-complexes and cation radical salts. These CT-complexes and radical salts were found to be metallic or semiconducting, reflecting the effect of stoichiometry control in the dimeric TTF system. The X-ray structures of two cation radical salts revealed a unique stacking, and the precise conducting path in BEDO-bi-TTF $\cdot$ ClO_4 was discussed on the basis of MO calculations. © 2002 Elsevier Science (USA)

Key Words: **tetrathiafulvalene; tetrathiafulvalene dimers; synthesis; X-ray analysis; redox properties; CT-complexes; radical salts; organic metals; MO calculations for conducting path.**

INTRODUCTION

Since the discovery of the properties of tetrathiafulvalene (TTF) in 1970 (1–3), much effort has been devoted to designing new analogues and counterparts of this π-donor in order to improve the electroconductive properties of the corresponding CT-complexes and radical salts (4–7). One important concept to realize high electric conductivity is the enhancement of the dimensionality, which can be attained by use of dichalcogen-capped TTF or by the extended π-conjugation of the TTF framework (8–11). Thus, a variety of dimeric TTF derivatives have been synthesized in which the two TTF groups are linked by σ-bonds, single chalcogen atoms, conjugated π-systems, or alkyl chains (8–10). Among them, bi-TTF **1** is a feasible candidate for constructing organic metals with high dimensionality based on a π-expanded donor. It provides an opportunity to control the stoichiometry, band filling, and molecular assembly in the desired conductive complexes (12). Although bi-TTF **1** was first reported in 1982 as an abstract of a conference, no physical and spectral data were presented (13). The second synthesis of **1** with spectral characterization was reported by Neilands *et al.* in 1989 using copper-catalyzed coupling of the Grignard reagent derived from a TTF diester, followed by decarboxylation with LiBr in HMPA (14). In the course of our studies on the synthesis of functional π-electron systems using transition-metal complexes (15), we planned an efficient synthesis of **1** by the palladium-catalyzed homo-coupling of trialkylstannyl-TTF which can be prepared from the commercially available TTF. Although **1** shows slightly higher oxidation potentials as compared to the parent TTF, the donor properties of **1** are sufficient to form organic metals. On the basis of these results, symmetrically and unsymmetrically substituted bi-TTFs **2**–**7** can be expected to be efficient donors for constructing organic metals with higher dimensionality.

Recently, dimeric TTFs can be regarded as building blocks in supramolecular chemistry, and large 'belt-shaped' molecules, cage molecules, and 'tweezers-like' molecules have been investigated in order to realize redox sensors, conducting organic magnets, and novel crystal structures (16–18). Although several methods for preparing dimeric TTFs have been reported, the synthetic methodology available for bi-TTFs was limited until now (19–22). Therefore, we first developed a new synthetic method of

[1]To whom correspondence should be addressed. Fax: +81-426-77-2525. E-mail: iyoda-masahiko@c.metro-u.ac.jp.

0022-4596/02 $35.00

bi-TTFs **1**–**7** using transition-metal-catalyzed coupling reactions, and then prepared CT-complexes and radical salts derived from **1** to **7**. In preliminary form, we reported the synthesis of bi-TTF **1** (23) and the conducting properties of CT-complexes and radical salts derived from **1**–**7** (24). In this paper we describe the details of the successful syntheses and structures of **1**–**7**, together with structures and high electric conductivities of their radical salts.

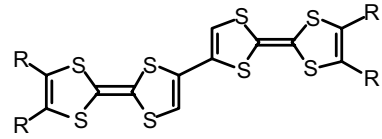

1: R = H **2**: R = SCH_3
3: R_2 = $S(CH_2)_2S$ **4**: R_2 = $O(CH_2)_2O$

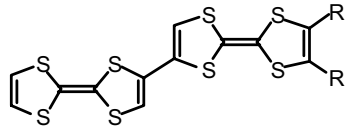

5: R = SCH_3 **6**: R_2 = $S(CH_2)_2S$
7: R_2 = $O(CH_2)_2O$

EXPERIMENTAL

General Procedure

^1H and ^{13}C NMR spectra were recorded on JEOL LA-500 and JEOL LA-400 instruments. Spectra are reported (in δ) referenced to Me_4Si. Unless otherwise noted, $CDCl_3$ was used as solvent. Data are reported as follows: chemical shifts, multiplicity (s = singlet, d = doublet, t = triplet, m = multiplet, br = broad), integration, and coupling constant (Hz). MS spectra were determined on a JEOL JMS-AX 500 instrument and KRATOS AXIMA-CFR. Only the more intense or structurally diagnostic mass spectral fragment ion peaks are reported. Melting points except for **1**–**4** were determined on a Yanaco Micro melting point apparatus MP-500D and are uncorrected. Melting points of **1**–**4** were determined by TG analysis with a Seiko Instrument SSC5200 under nitrogen atmosphere (heating rate 5 K/min). Elemental analyses were performed in the microanalysis laboratory of Tokyo Metropolitan University. Column chromatography was carried out with use of EM Reagents silica gel 60, 70–230 mesh ASTM, Daiso silica gel 1001 W, or neutral alumina activity II–III, 70–230 mesh ASTM. Gel permeation liquid chromatography (GLPC) was performed on AL LC-08 and LC-918 liquid chromatography instruments with JAIGEL-1 H column (20 mm × 600 mm × 2) and chloroform as eluent. All solvents were dried by conventional procedures. BMT-TTFI **13** (25), EDT-TTFI **14** (26), and EDO-TTF **15** (27) were prepared using the published procedures.

Synthesis of 4-Trimethylstannyltetrathiafulvalene (8, TTFSnMe_3)

To a solution of TTF (300 mg, 1.47 mmol) in THF (5 ml) was added dropwise over 7 min a hexane solution of *n*-BuLi (1.53 M, 1.0 ml, 1.5 mmol) at –78°C under argon atmosphere. The mixture was stirred at the same temperature for 1 h, and a solution of Me_3SnCl (480 mg, 2.41 mmol) in THF (2 ml) was added at –78°C over a period of 10 min. The mixture was stirred at the same temperature for 1 h, and then was warmed slowly to room temperature. After stirring at room temperature for 1 h, the mixture was diluted by addition of hexane (150 mL). The mixture was filtered through Hyflo Super Cel. The filtrate was concentrated in vacuo to afford **8** (462 mg, 86%) as a yellow oil. EI-MS *m/z* 348 (M^+); ^1H NMR (500 MHz) δ 0.343 (s, 9 H), 6.147 (s, 1 H), 6.281 (d, J = 6.5 Hz, 1 H), 6.291 (d, J = 6.5 Hz, 1 H).

Synthesis of 4-Trimethylstannyltetrathiafulvalene Derivatives (9–11)

In a manner similar to the synthesis of **8**, 4-trimethylstannyltetrathiafulvalene derivatives **9**, **10**, and **11** were prepared from 4,5-bis(methylthio)tetrathiafulvalene (BMT-TTF), 4,5-ethylenedithiotetrathiafulvalene (EDT-TTF), and 4,5-ethylenedioxytetrathiafulvalene (EDO-TTF) in 48%, 55%, and 29% yields, respectively. **9**: orange oil, ^1H-NMR (400 MHz) δ 0.337 (s, 9 H), 2.422 (s, 6 H), 6.331 (s, 1 H). **10**: orange oil, ^1H-NMR (500 MHz) δ 0.330 (s, 9 H), 3.267 (s, 4 H), 6.351 (s, 1 H). **11**: orange oil, ^1H NMR (500 MHz) δ 0.375 (s, 9 H), 4.251 (s, 4 H), 6.334 (s, 1 H).

Synthesis of 4′,4″-Bitetrathiafulvalene (bi-TTF, 1) by the Coupling of 8 with $Cu(NO_3)_2 \cdot 3H_2O$

To a solution of **8** (270 mg, 0.738 mmol) in THF (8 ml) was added a solution of $Cu(NO_3)_2 \cdot 3H_2O$ (195 mg, 0.807 mmol) in THF (2 mL) under argon atmosphere. The mixture was stirred at ambient temperature for 70 min, and was diluted by addition of CS_2 (150 mL). The mixture was passed through a short column of deactivated alumina containing 30% water. The eluent was concentrated in vacuo to give a residue which was chromatographed on silica gel with CS_2 as eluent to afford bi-TTF **1** (111 mg, 74%) as orange leaflets, mp 217°C (decomp.) based on TG analysis, EI-MS *m/z* 406 (M^+); ^1H NMR (500 MHz, $CDCl_3$–CS_2 1:1) δ 6.116 (s, 2H), 6.269 (s, 4H); ^{13}C NMR (125 MHz, $CDCl_3$-CS_2 1:1) δ 100.3, 114.4, 118.2, 118.98, 119.00, 127.1.

Synthesis of 4,5,4‴,5‴-Tetrakis(methylthio)-4′, 4″-Bitetrathiafulvalene (TMT-bi-TTF, 2) by the Coupling of 9 with $Pd(OAc)_2$

To a suspension of $Pd(OAc)_2$ (77.5 mg, 0.321 mmol) in benzene (3 mL) was added a solution of **9** (221 mg, 0.482 mmoL) under argon atmosphere. The mixture was stirred at ambient temperature for 2 h, and then diluted with CS_2 (130 mL). The mixture was passed through a short column of deactivated alumina containing 30% water. The eluent was concentrated in vacuo to give a residue which was chromatographed on silica gel with CS_2 as eluent to afford TMT-bi-TTF **2** (61 mg, 43%) as red needles, mp 167°C based on TG analysis, FAB-MS *m/z* 588 (M^+); ^{1}H NMR (500 MHz) δ 2.394 (s, 12H), 6.142 (s, 2H); ^{13}C NMR (125 MHz) δ 19.25, 110.3, 112.1, 118.0, 126.9, 127.6, 127.7.

Synthesis of 1, 3, and 4 by the Coupling of 8, 10, and 11 with $Pd(OAc)_2$

In a manner similar to the synthesis of **2** with $Pd(OAc)_2$, bi-TTFs (**1**, **3**, and **4**) were synthesized by the reaction of the corresponding trimethyltin-TTF derivatives (**8**, **10**, and **11**) with $Pd(OAc)_2$ in benzene in 67%, 43%, and 47% yields, respectively.

Compound **3**, red fine crystals, mp 185°C (decomp) based on TG analysis, FAB-MS *m/z* 586 (M^+); ^{1}H-NMR (500 MHz, $CDCl_3$–CS_2 1:1) δ 3.272 (s, 8H), 6.136 (s, 2H). **4**, red fine crystals, mp 183°C (decomp) based on TG analysis, FAB-MS *m/z* 522 (M^+); ^{1}H NMR (500 MHz, $CDCl_3$–CS_2 1:1) δ 4.230 (s, 8H), 6.166 (s, 2H).

Synthesis of 1, 2, and 3 by the Homo-Coupling of 12, 16, and 17 with $PdCl_2(PPh_3)_2$

To a solution of TTF (207 mg, 1.01 mmol) in THF (5 mL) was added dropwise over 7 min a hexane solution of *n*-BuLi (1.53 M, 0.7 mL, 1.07 mmol) at –78°C under argon atmosphere, and the mixture was stirred at the same temperature for 1 h. A solution of zinc chloride (163 mg, 1.20 mmol) in THF (3 ml) was added dropwise at –78°C, and the mixture was stirred at the same temperature for 1 h. The mixture was allowed to warm to −10°C, and then $PdCl_2(PPh_3)_2$ (352 mg, 0.501 mmol) was added to the mixture. The mixture was warmed to room temperature, stirred at the same temperature for 1 h, and then diluted by addition of CS_2 (200 mL). The mixture was passed through a short column of deactivated alumina containing 30% water. The eluent was concentrated in vacuo to give a residue which was chromatographed on silica gel with CS_2 as eluent to afford bi-TTF **1** (103 mg, 50%), together with the recovered TTF (27 mg, 13%).

In a similar manner, **2** and **3** were prepared from BMT and EDT-TTF in 70% and 80% yields, respectively.

Synthesis of 5–7 by the Cross-Coupling of 12 with 13–15

A hexane solution of *n*-BuLi (1.53 M, 0.7 mL, 1.07 mmol) was added dropwise over 7 min to a solution of TTF (207 mg, 1.01 mmol) in THF (5 mL) at –78°C under argon atmosphere, and the mixture was stirred at the same temperature for 1 h. A solution of zinc chloride (163 mg, 1.20 mmol) in THF (3 mL) was added dropwise at –78°C, and the mixture was stirred at the same temperature for 1 h. The mixture was allowed to warm to −10°C, and a solution of **13** (206 mg, 0.487 mmol) and $Pd(PPh_3)_4$ (116 mg, 0.1 mmol) in THF (5 mL) were added. The mixture was stirred at –10°C for 1 h and then at room temperature for 1 h, and evaporated in vacuo. The residue was passed through a short column of deactivated alumina containing 30% water using CS_2 as eluent. The eluent was concentrated in vacuo to give crude products which were chromatographed on silica gel with CS_2 as eluent to afford **5** (170 mg, 70%) as yellow powder, mp 166.5–167.5°C (decomp), TOF-MS *m/z* 498 (M^+); ^{1}H NMR (500 MHz) δ 2.428 (s, 3H), 2.432 (s, 3H), 6.220 (s, 2H), 6.329 (d, J = 6.5 Hz, 1H), 6.337 (d, J = 6.5 Hz, 1H).

In a similar manner, **6** and **7** were prepared by the cross coupling of **12** with **14** and **15** in 80% and 20% yields, respectively. **6**: red plates, mp 201.0–202.5°C (decomp), TOF-MS *m/z* 496 (M^+); ^{1}H-NMR (500 MHz) δ 3.290 (s, 4H), 6.172 (s, 1H), 6.186 (s, 1H), 6.302 (s, 2H); ^{13}C NMR (125 MHz) δ 30.26, 107.10, 108.34, 113.74, 113.77, 114.52, 117.74, 118.38, 118.93, 118.95, 126.90, 126.91. **7**: red needles, TOF-MS *m/z* 464 (M^+); ^{1}H NMR (500 MHz) δ 4.231 (s, 4H), 6.108 (s, 1H), 6.203 (s, 1H), 6.284 (m, 2H).

X-Ray Structural Determination of 2, 4, $2 \cdot ClO_4$, and $4 \cdot ClO_4$

Crystals of **2** and **4** suitable for X-ray structure analysis were obtained by slow recrystallization of **2** and **4** from CS_2, respectively. Crystals of $\mathbf{2} \cdot ClO_4$ and $\mathbf{4} \cdot ClO_4$ were obtained by the galvanostatic oxidation (ca. 1 μA) of **2** and **4** with $Bu^n_4NClO_4$ in THF, respectively. Intensity data were collected using a Rigaku AFC7R four-circle diffractometer with graphite-monochromated Mo$K\alpha$ radiation (λ = 0.71069 Å). Structural parameters of non-hydrogen atoms were refined anisotropically and some hydrogen atoms were refined isotropically according to the full-matrix least-squares technique. The results are summarized in Table 1.

The intermolecular overlap integrals are calculated on the basis of the extended Hückel molecular orbital calculations (28). From the calculated overlap integrals,

TABLE 1
Crystallographic Data of Bi-TTF Derivatives (2 and 4) and Their Cation Radical Salts ($2 \cdot ClO_4$ and $4 \cdot ClO_4$)

Compound	**2** (TMT-bi-TTF)	**4** (BEDO-bi-TTF)	$2 \cdot ClO_4$	$4 \cdot ClO_4$
Empirical formula	$C_{16}H_{14}S_{12}$	$C_{16}H_{10}O_4S_8$	$C_{16}H_{14}ClO_4S_{12}$	$C_{16}H_{10}ClO_8S_8$
Formula weight	591.01	522.73	690.46	622.18
Crystal color	Red	Red	Black	Black
Crystal dimension (mm^3)	$0.06 \times 0.06 \times 0.25$	$0.30 \times 0.10 \times 0.25$	$0.15 \times 0.04 \times 0.20$	$0.08 \times 0.15 \times 0.22$
Crystal system	Monoclinic	Monoclinic	Triclinic	Triclinic
Cell parameters				
a (Å)	4.124(1)	5.104(2)	12.228(3)	9.937(2)
b (Å)	19.003(4)	7.522(2)	13.112(2)	13.685(2)
c (Å)	16.942(3)	25.888(2)	8.838(2)	8.431(3)
α (°)	90	90	103.66(2)	94.18(2)
α (deg)	94.00(2)	91.61(3)	105.59(2)	97.37(2)
β (deg)	90	90	74.44(2)	100.32(1)
V ($Å^3$)	1324.4(5)	933.4(4)	1294.2(5)	1113.2(5)
Space group	$P2_1/n$	$P2_1/n$	P-1	P-1
Z-value	2	2	2	2
D_{calc} (g/cm^3)	1.482	1.747	1.772	1.856
$F(000)$	604.00	532.00	702.00	630.00
μ(Mo$K\alpha$)	9.93	9.21	11.41	9.67
$2\theta_{max}$ (deg)	55.0	55.0	55.0	55.0
Unique reflections	3153	2473	5935	4167
Observed reflections ($I > 3\sigma(I)$)	1138	1618	2389	1371
Residuals: R; R_w	0.069; 0.102	0.031; 0.028	0.048; 0.055	0.048; 0.048

the energy band is calculated according to the tight-binding approximation.

Cyclic Voltammetry

All electrochemical studies were performed using a BAS CV-27 voltammetric analyzer, which was equipped with a platinum electrode (1.6 or 3 mm diameter) as a working electrode, a standard Ag/Ag^+ reference electrode and a platinum wire counter-electrode. The measurements were carried out on degassed anhydrous benzonitrile solution containing the sample (0.5–1 mM) and tetrabutylammonium perchlorate (0.1 M) as supporting electrolyte at 296 K. Cyclic voltammograms were scanned at a sweep rate of 100 mV/s. Oxidation potentials are referred to ferrocene; $Cp_2Fe^{+/0}$ was set to 0.46 V which corresponds to the potential vs SCE.

RESULTS AND DISCUSSION

Synthesis of bi-TTFs

The lithiated TTF monoanions generated from TTF and its derivatives with 1 equiv of Bu^nLi at low temperatures can be easily transformed into organotin (**8**–**11**) and zinc derivatives (**12**) by treatment with chlorotrimethyltin(IV) and zinc chloride, respectively (Scheme 1). As summarized in Table 2, $TTFSnMe_3$ **8** reacts with $Cu(NO_3)_2 \cdot 3H_2O$ or $Pd(OAc)_2$ in THF or benzene at room temperature to produce the corresponding homo-coupling product **1** in 70% or 67% yields, respectively. Although $Cu(NO_3)_2 \cdot 3H_2O$ is an effective reagent for the coupling of **8**, the substituted $TTFSnMe_3$ **9**–**11** and the coupling products **2**–**4** decomposed rapidly under similar conditions. Therefore, the reactions of **9**–**11** with stoichiometric amounts of $Pd(OAc)_2$ were employed for the synthesis of **2**–**4**. The palladium(II)-mediated homo-coupling of **9**–**11** afforded the corresponding bi-TTFs **2**–**4** in 43–47% yields, respectively. All reactions form hydrolyzed products, i.e., the starting TTF and its derivatives, which can be used again for the synthesis of the organotin compounds **8**–**11**.

A reddish-brown solution of TTFZnCl **12** is prepared from the monolithiated TTF with 1.2 equiv of anhydrous $ZnCl_2$ in THF, and **12** can be expected to be a versatile reagent. Although TTFLi is unstable at 0°C to dispropor-

TABLE 2
Transition-Metal-Catalyzed Homo-Coupling of 8–11

Compound	Metal catalyst	Solvent	Time (h)	Product	Yield (%)
8	$Cu(NO_3)_2 \cdot 3H_2O$	THF	1	**1**	70
8	$Pd(OAc)_2$	Benzene	2	**1**	67
9	$Pd(OAc)_2$	Benzene	2	**2**	43
10	$Pd(OAc)_2$	Benzene	2	**3**	43
11	$Pd(OAc)_2$	Benzene	2	**4**	47

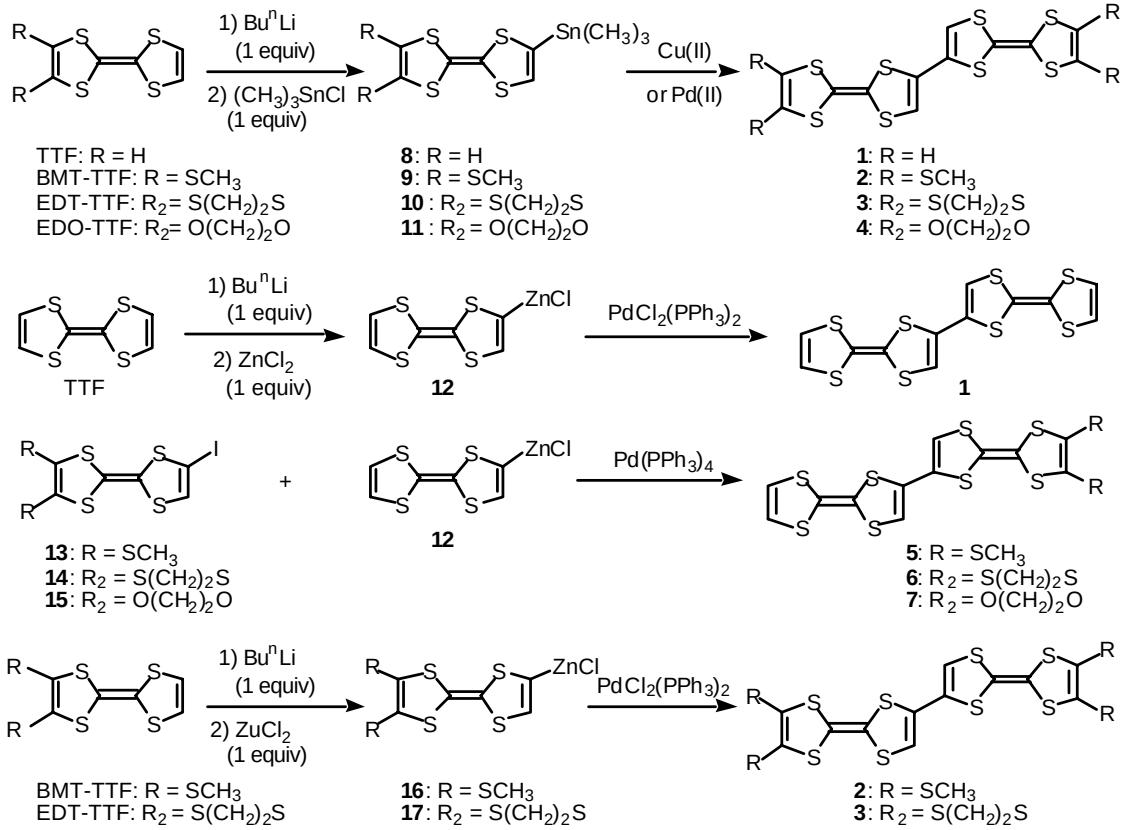

SCHEME 1. Syntheses of symmetrical and unsymmetrical bi-TTFs 1–4 and 5–7.

tionate TTF and $TTFLi_2$ (29), **12** is stable at 0°C in solution and shows no decomposition or disproportionation. Thus, TTFZnCl **12** can be successfully employed for both palladium-catalyzed homo- and cross-coupling reactions. As shown in Scheme 1, 0.5 equiv of $PdCl_2(PPh_3)_2$ was added to a solution of **12** in THF at −78°C, and the resulting solution was stirred at −10°C for 1 h and then at room temperature for 1 h to produce bi-TTF **1** in 57% yield based on the consumed TTF (13% of the recovered TTF). Similarly, the homo-coupling of zinc species **16** and **17** with $PdCl_2(PPh_3)_2$ afforded **2** and **3** in 70% and 80% yields, respectively. For the cross-coupling, the reaction of **12** (1.7–2 equiv) with the iodo-TTF derivative **13**–**15** (1 equiv) in THF in the presence of $Pd(PPh_3)_4$ (10 mol%) at −10 °C for 1 h and then at room temperature for 1 h led to the unsymmetrical bi-TTF **5**, **6**, and **7** in 88%, 70%, and 20% yields, respectively. The low yield of **7** is presumably due to the difficulty in isolating the product from the reaction mixture.

Crystal Structures of Bi-TTFs

The structures of **2** and **4** have been determined by X-ray analysis. As shown in Figs. 1(a) and 2(a), **2** and **4** have a crystallographic S_2 symmetry and the two-fold axes passing through the C(1)–C(1*) bonds between two TTF units. Thus, the central $S_2C_2S_2$ moieties are exactly planar, and both molecules have an almost planar structure with a zigzag conformation [Figs. 1(b) and 2(b)]. The X-ray analysis of **1** by Becker *et al*. indicates a similar molecular structure (20). The crystal structures of **2** and **4** shown in Figs. 1(c) and 2(c) are characterized by a slipped plane-to-plane stacking, and the face-to-face distances between the molecular planes are 3.61 and 3.62 Å, respectively. In contrast to the face-to-face stacking of **2** and **4**, **1** shows an edge-to-face arrangement in the crystal (20). There are intermolecular S···S distances less than the sum of the van der Waals radii [S(2)···S(5) = 3.480 and S(1*)···S(6) = 3.629 Å in **2**; S(2)···S(3) = 3.520(1) Å in **4**].

Redox Behavior of Bi-TTFs

The oxidation potentials of **1**–**4**, **5**–**7**, TTF, BMT-TTF, EDT-TTF, and EDO-TTF measured by cyclic voltammetry are shown in Table 3. Although the solubility of **3** and **4** is rather low in common organic solvents, well-assignable voltammograms were obtained in benzonitrile as the solvent (Fig. 3). As shown in Table 3, the parent bi-TTF

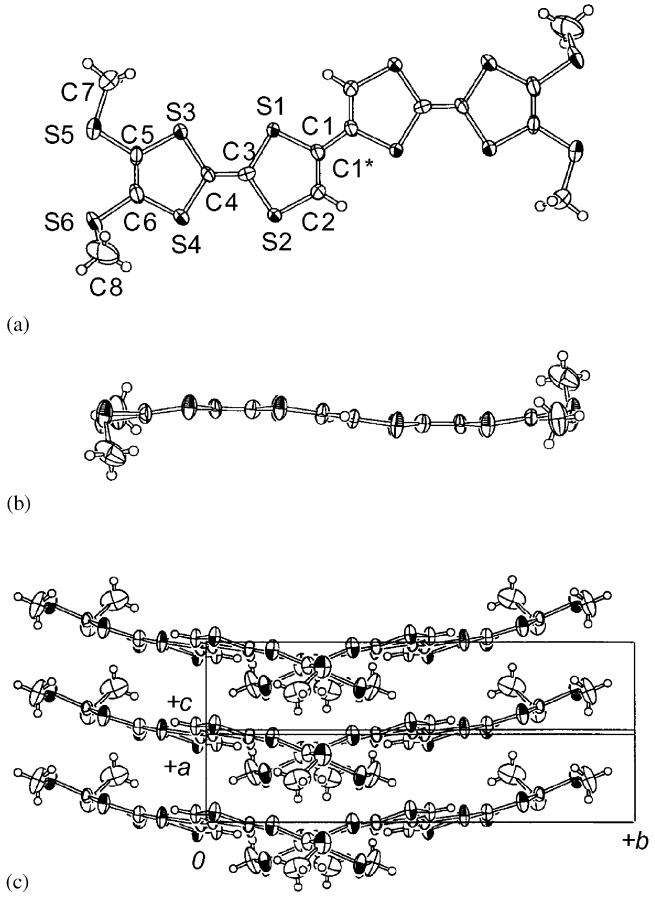

FIG. 1. X-ray structure of TMT-bi-TTF **2**: (a) view of the best molecular plane, (b) view perpendicular to that shown in (a), (c) crystal structure. Selected distances (Å) for **2** are as follows: S(1)–C(1) 1.76(1), S(1)–C(3) 1.76(1), S(2)–C(2) 1.73(1), S(2)–C(3) 1.75(1), C(1)–C(1)* 1.43(2), C(1)–C(2) 1.37(1), C(3)–C(4) 1.34(1).

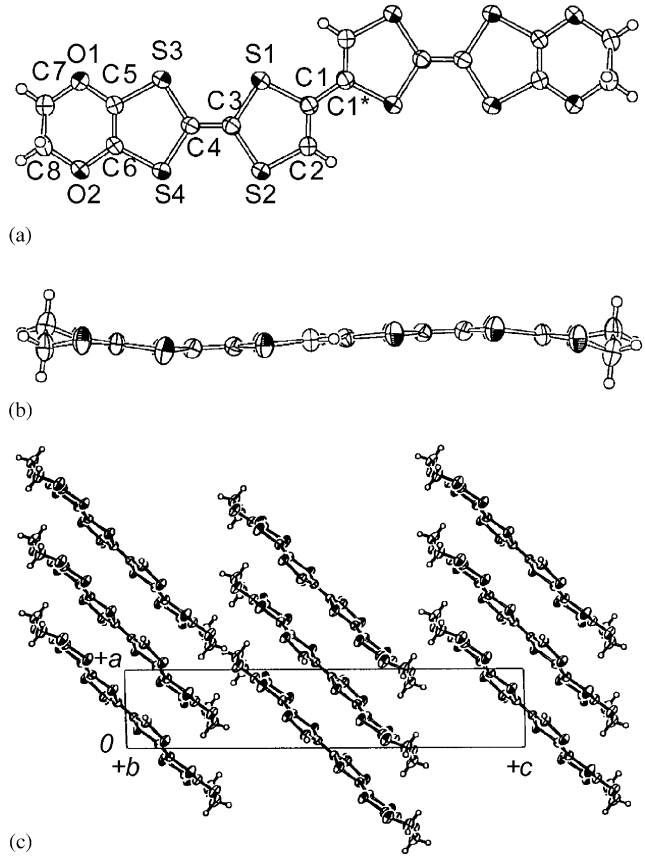

FIG. 2. X-ray structure of BEDO-bi-TTF **4**: (a) top view of the molecule, (b) view perpendicular to that shown in (a), (c) crystal structure. Selected distances (Å) for **4** are as follows: S(1)–C(1) 1.759(3), S(1)–C(3) 1.758(2), S(2)–C(2) 1.730(3), S(2)–C(3) 1.751(3), C(1)–C(1)* 1.441(4), C(1)–C(2) 1.337(3), C(3)–C(4) 1.331(3).

1 shows two redox waves in benzonitrile, whereas the reported oxidation of **1** in acetonitrile is a three-step process (14, 20). By contrast, **2**–**4** and **5**–**7** show three redox waves, in which the third redox process seems to be two-electron oxidation. As shown in Fig. 3(a), the cyclic voltammogram of **1** shows a very broad first oxidation, reflecting the overlap of two closely located oxidations in benzonitrile. 4-Phenyl-TTF (**18**) shows a slightly higher first oxidation potential ($E^1_{1/2} = 0.38$ V) than that of TTF ($E^1_{1/2} = 0.36$ V) (23), whereas bi-TTF **1** has a much higher first oxidation potential ($E^1_{1/2} = 0.43$ V) than that of TTF, presumably due to larger electron-withdrawing effect of the TTF moiety as compared to the phenyl group. Although the bond formation between two TTF molecules at the 4-position causes the first oxidation potentials to shift positive by 0.03–0.12 V, the oxidation potentials ($E^1_{1/2}$) of **1**–**7** are much lower than that ($E^1_{1/2} = 0.55$ V) of BEDT-TTF which is a well-known donor. Therefore, bi-TTFs **1**–**7** can be expected to show good donor ability.

The redox behavior of bi-TTFs suggests that the through-bond interaction between the two TTF units is weak in the neutral, cation radical, and dicationic species of bi-TTFs (30), although the face-to-face through-space

TABLE 3
Redox Potentials of 1–7, 18, and Related Compounds in Benzonitrile

Compound	$E^1_{1/2}$	$E^2_{1/2}$	$E^3_{1/2}$
TTF	0.36	0.77	
BMT-TTF	0.44	0.77	
EDT-TTF	0.45	0.81	
EDO-TTF	0.39	0.76	
1	0.43	0.84	
2	0.52	0.63	0.87
3	0.52	0.62	0.87
4	0.46	0.55	0.87
5	0.47	0.62	0.86
6	0.46	0.68	0.89
7	0.42	0.54	0.86
18	0.38	0.80	

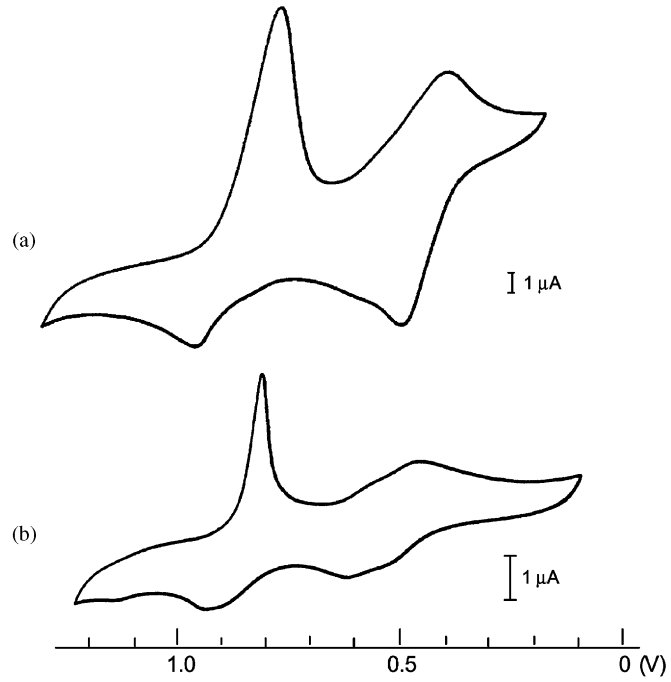

FIG. 3. Cyclic voltammograms of **1** (a) and **3** (b) in benzonitrile at 296 K.

interaction between the two TTF units is strong enough to form a mixed-valence state in either the cation radical or dicationic species (31). The weak interaction in the cation radicals of **1**–**7** results in the formation of small (or non) [class I] or slightly [class II] delocalized state (32), whereas the cation radical derived from the face-to-face fixed bi-TTF such as 1,8-bis(tetrathiafulvalenyl)naphthalene forms a strongly delocalized [class III] species (31). In the electrochemical oxidation of **1**–**7**, π-dimer formation or aggregation of cation radicals and dications can be excluded due to low solubility of **1**–**7** in benzonitrile (33). Experiments and calculations suggest that the cation radical $\mathbf{19}^{\cdot +}$ derived from hexamethylthio-bi-TTF **19** seems to possess a class I state (34), presumably due to its nonplanar structure with the torsion angle of 77° around the central σ-bond (22).

The ab initio calculations on **1**–**4** show that the molecular orbitals of bi-TTFs are spread over the whole molecules, and the first oxidation potentials and the HOMO levels bear a linear relationship to each other (35). Although **1** shows two two-electron oxidations, the first potential may be regarded as two one-electron oxidations.

Electrical Conductivities of CT-Complexes and Radical Salts

The dimeric TTFs **1**–**4** formed CT-complexes and cation-radical salts, but the unsymmetric **5**–**7** decomposed gradually under oxidation conditions. Therefore, the conducting behavior of the CT complexes and radical-cation salts derived from **1**–**4** has been investigated. As expected from the oxidation potentials in Table 3, **1** and **4** formed CT-complexes with TCNQ, whereas **2** and **3** formed those with DDQ. The radical-cation salts were prepared by electrochemical oxidation of **1**–**4** in a suitable solvent containing the corresponding tetrabutylammonium salt. As shown in Table 4, the CT-complexes derived from **1** and **4** with TCNQ showed fairly high room-temperature conductivities (4.8 and 3.6 S/cm), respectively, and $\mathbf{1} \cdot$TCNQ was metallic down to 160 K. However, the **3**-DDQ-complex is a semiconductor (0.84 S/cm). Although the I_3^- salt of **1** and the ClO_4^- salt of **2** were semiconductors, the I_3^-, AuI_2^- and BrI_2^- salts of **3** exhibited high conductivities (125, 778 and 80 S/cm) with metallic behavior down to 240, 285, and 240 K, respectively, being transformed at lower temperature to semiconductors with small activation energies. Furthermore, the ClO_4^- salt of **4** indicated semiconductive resistive temperature dependence (6.9 S/cm) with a small activation energy (35 meV), whereas the I_3^- salt of **4** was metallic (8.0 S/cm) at room temperature. As shown in Fig. 4, $\mathbf{4}_3 \cdot I_3$ showed a metallic behavior at 300 K and a semi-metallic conductivity down to 135 K, exhibiting a typical temperature dependence of resistivity for the cation-radical salts of bi-TTFs.

Combination of dimeric donors and acceptors has been expected to lead to a 1:1 stoichiometry of CT-complexes and radical ion salts with an interesting double Fermi surface (12). Thus, $\mathbf{1} \cdot$TCNQ, $\mathbf{2} \cdot ClO_4$, $\mathbf{3} \cdot AuI_2$, $\mathbf{3} \cdot BrI_2$, and $\mathbf{4} \cdot ClO_4$ consist of the 1:1 stoichiometry. If we assume each TTF moiety to be independent, the band may be 3/4 filled. In the case of $\mathbf{1} \cdot$TCNQ, the degree of charge transfer (Z) is estimated at 0.7 based on the IR measurement, and hence a

TABLE 4
Electrical Conductivities of CT-Complexes and Radical-Cation Salts Derived from 1–4

Donor	Acceptor	Solvent	D:A[a]	σ_{rt}(S/cm)[b]	
1	TCNQ	PhCl	1:1	4.8	(metallic)
1	I_3	TCE[c]	3:2	7.6	
2	ClO_4	THF	1:1[d]	9.4×10^{-2}	
3	DDQ	Benzene	2:1	8.4×10^{-1}	
3	I_3	THF	2:1	125	(metallic)
3	AuI_2	THF	1:1	778	(metallic)
3	BrI_2	PhCl	1:1	80	(metallic)
4	TCNQ	PhCl	3:1	3.6	(E_a = 72 meV)
4	ClO_4	THF	1:1[d]	6.9	(E_a = 35 meV)
4	I_3	PhCl	3:1	8.0	(metallic)

[a] Determined by elemental analysis.
[b] Room-temperature conductivity measured on a single crystal by a four-probe technique.
[c] 1,1,2-Trichloroethane.
[d] Determined by X-ray analysis.

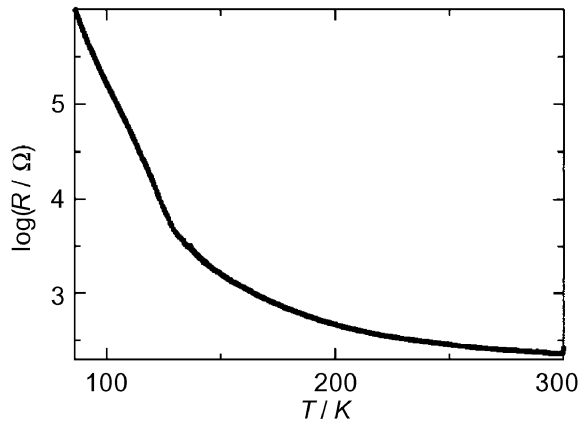

FIG. 4. Temperature dependence of the resistivity for $\mathbf{4}_3 \cdot (I_3)$.

higher band filling (0.825) can be expected in $\mathbf{1} \cdot$TCNQ. In contrast, the I_3^- salt of **1** is made up of the 3:2 stoichiometry, and the DDQ complex of **2** and the I_3^- salt of **3** consist of the 2:1 stoichiometry. Thus, the formal charge transfers in these compounds are 1/6 and 1/8, respectively, for one TTF unit. Furthermore, the TCNQ-complex and I_3 salt of **4** are composed of the 3:1 stoichiometry, the formal charge-transfer being 1/12 for one TTF unit, although the crystal structures of these compounds are unknown so far. Since bi-TTFs **1**–**4** resulted in the formation of the donor-rich CT-complexes and radical ion salts selectively, the stoichiometry control can be easily achieved using these dimeric TTFs to form a new type of organic metals with preferable donor–acceptor ratio.

Crystal Structures and Intermolecular Interactions of the Radical Salts

In order to clarify the crystal packings of novel radical salts derived from **1**–**4**, the crystal structures of $\mathbf{2} \cdot ClO_4$ and $\mathbf{4} \cdot ClO_4$ were determined by the X-ray diffraction method. As shown in Figs. 5–7, the radical ion salts of **2** and **4** show unique crystal packings, reflecting a dimeric TTF structure. The net charge on a donor molecule is expected to be $+1$ due to the 1:1 composition, the charge being half-full in each TTF unit (the band is 3/4 filled). The bi-TTF frameworks in $\mathbf{2} \cdot ClO_4$ and $\mathbf{4} \cdot ClO_4$ exhibit slightly bent and planar structures, the maximum atomic deviations from the least-squares plane of the bi-TTF units excepting the substituents being 0.46 and 0.18 Å, respectively.

As shown in Fig. 5, the TMT-bi-TTF molecules are stacked face-to-face to form a dimeric structure (Fig. 5(a)), and the dimers are arranged in the so-called β'-type structure to form a conducting along the *c*-axis. There are four intra- and interstack interactions between the cation radicals (Fig. 5(a)) and Table 5). Although $\mathbf{2} \cdot ClO_4$ has a semiconducting property (9.4×10^{-2} S cm), we

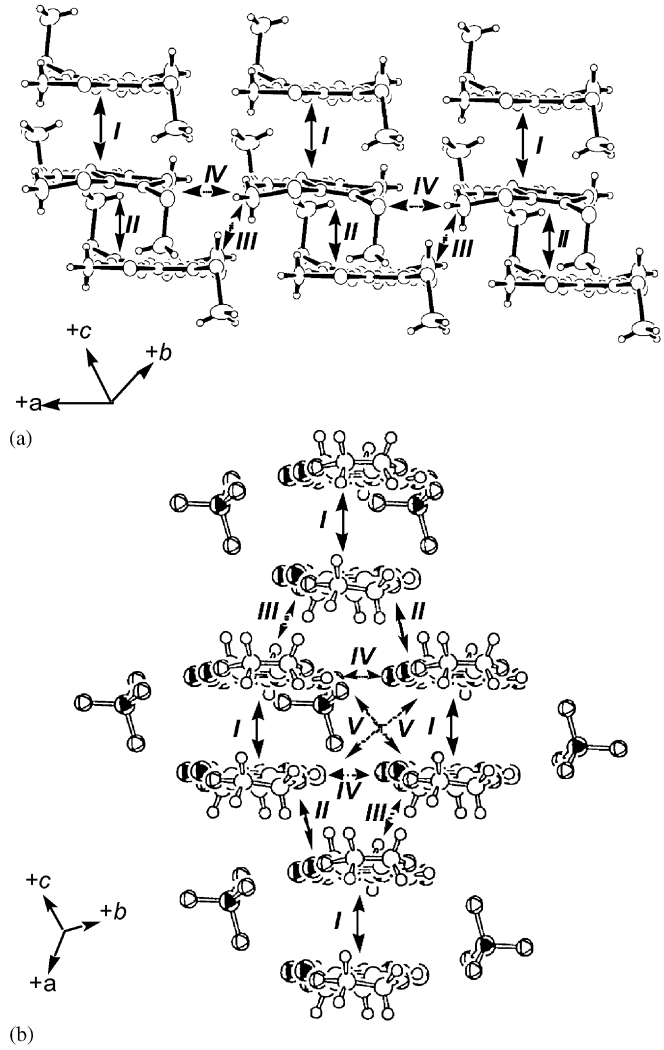

FIG. 5. The intra- and interstack overlaps of cation radicals in $\mathbf{2} \cdot ClO_4$ and $\mathbf{4} \cdot ClO_4$. The inter-columnar S···S or S···O distances indicated by dotted lines and the intracolumn short S···S contacts indicated by solid lines. (a) The overlaps (I–IV) in $\mathbf{2} \cdot ClO_4$. The ClO_4 anions have been removed for clarity. (b) Overlaps (I–V) in $\mathbf{4} \cdot ClO_4$.

examined the structure of $\mathbf{2} \cdot ClO_4$ based on the X-ray and overlap integral analyses (Figs. 5(a) and 6). Since the C(3)–C(4) (1.394(9) Å) and C(11)–C(12) (1.343(9) Å) bonds have single and double bond character, respectively, the two TTF units in $\mathbf{2} \cdot ClO_4$ have a different oxidation state, i.e., cation radical and neutral states on the right (B) and left (A) halves of molecules (Fig. 6(a)). The two face-to-face distances observed between TMT-bi-TTFs along the *c*-axis (Figs. 6(b) and (c)) are 3.50 and 3.55 Å, corresponding to the two overlaps (II and I), respectively. There are two types of side-by-side interactions between TMT-bi-TTFs, one of which is strong (IV in Fig. 6(c)), whereas the other is weak (III in Fig. 6(b)). Thus, each cation radical

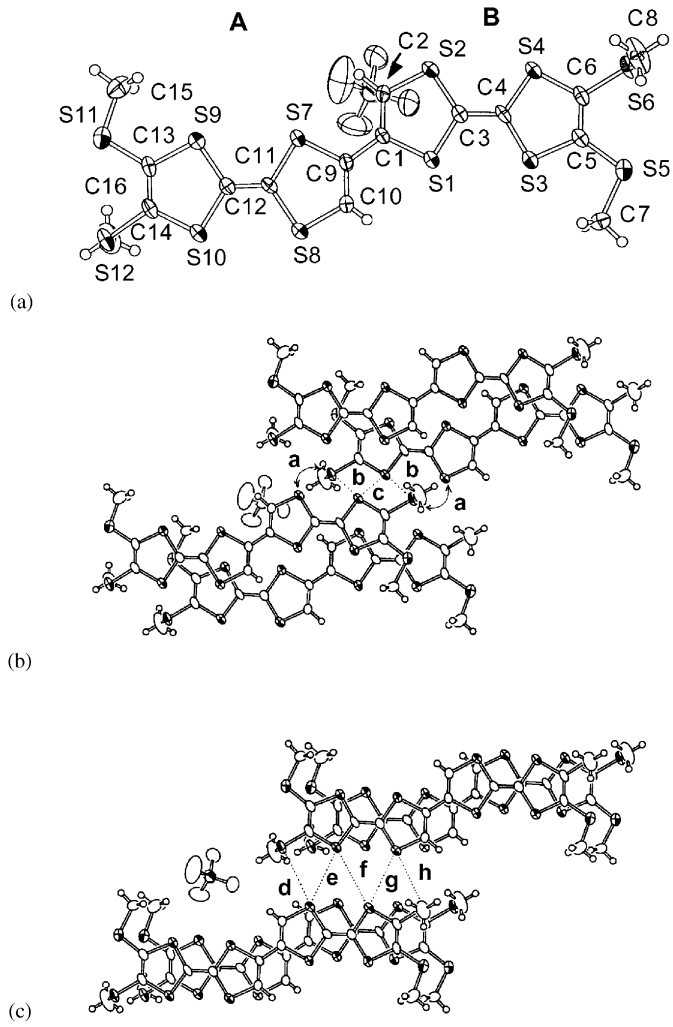

FIG. 6. X-ray structure and interstack overlaps of cation radical $\mathbf{2}\cdot ClO_4$: (a) top view of the molecule, (b) Overlaps II and III in Fig. 5(a); inter-columnar S···S distances (a = 3.91 Å, b = 3.79 Å, c = 3.97 Å) with 3.55 Å of the face-to-face stacking, (c) Overlaps I and IV in Fig. 5(a); inter-columnar S···S distances (d = 3.64, e = 3.57, f = 3.79, g = h = 3.50 Å) with 3.50 Å of the face-to-face stacking. Selected distances (Å) for $\mathbf{2}\cdot ClO_4$ are as follows: S(1)–C(1) 1.755(7), S(1)–C(3) 1.729(7), S(2)–C(2) 1.710(7), S(2)–C(3) 1.724(7), S(3)–C(4) 1.712(8), S(3)–C(5) 1.747(7), S(4)–C(4) 1.719(7), S(4)–C(6) 1.729(7), S(7)–C(9) 1.751(7), S(7)–C(11) 1.762(6), S(8)–C(10) 1.732(7), S(8)–C(11) 1.755(7), S(9)–C(12) 1.754(7), S(9)–C(13) 1.759(7), S(10)–C(12) 1.751(7), S(10)–C(14) 1.755(7), C(1)–C(2) 1.363(9), C(3)–C(4) 1.394(9), C(5)–C(6) 1.363(9), C(1)–C(9) 1.449(8), C(9)–C(10) 1.330(9), C(11)–C(12) 1.343(9), C(13)–C(14) 1.345(9).

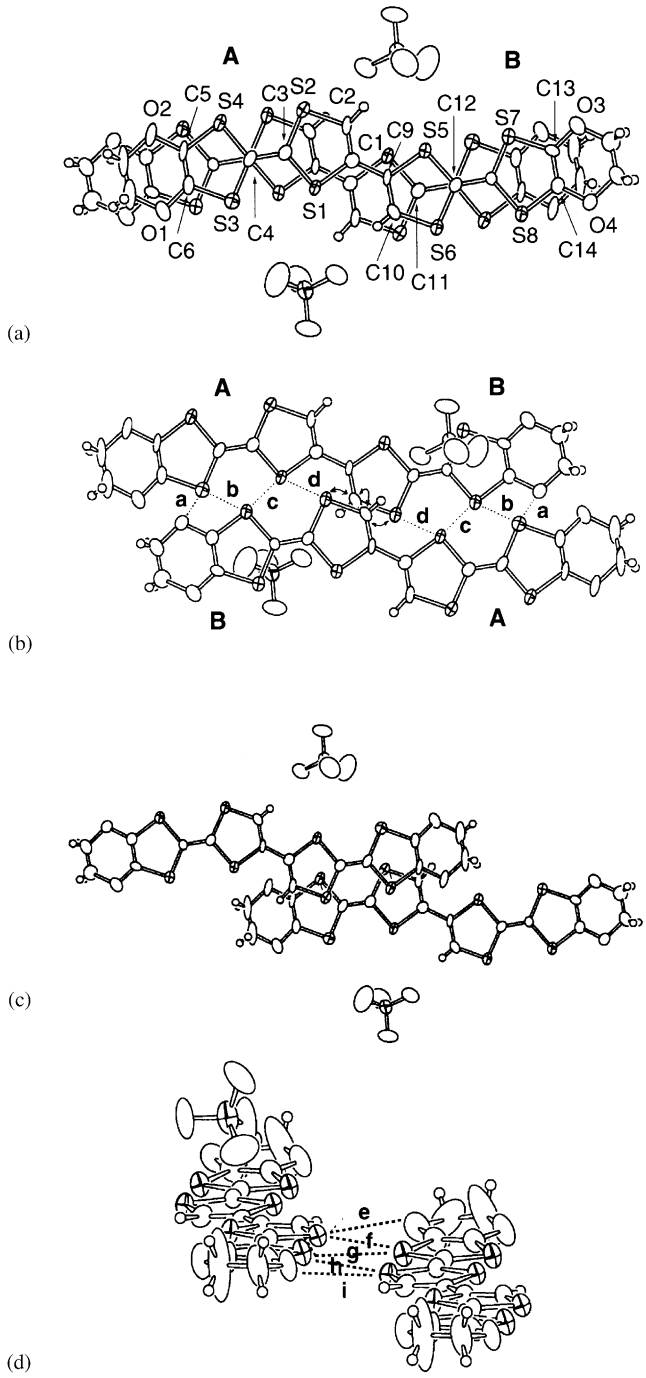

FIG. 7. The intra and interstack overlaps in $\mathbf{4}\cdot ClO_4$: (a) overlap I in Fig. 5(b); the atomic numbers and the two TTF parts (A and B) belong to the upper molecule, (b) overlap II in Fig. 5b and inter-columnar S···S and S···O distances (a = 3.48, b = 3.78, c = 3.70, d = 3.83 Å), (c) the overlap III in Fig. 5(b) and intra-column short S···S contacts (3.69 Å) indicated by solid lines. (d) Overlap IV in Fig. 5(b) and inter-columnar S···S and S···O distances (e = 3.36, f = 3.45, g = 3.59, h = 3.46, i = 3.41 Å).

unit and the neutral unit in $\mathbf{2}\cdot ClO_4$ form a column structure, and the former shows strong side-by-side interaction (IV in Figs. 5(a) and 6(c)). The calculated overlap integrals are listed in Table 5. In these calculations, the two TTF parts (A and B in Fig. 6(a)) of a single molecule are treated as if these are two independent molecules, although the corresponding molecular orbitals are originally HOMO and the next HOMO. Thus, each of the I–IV interactions in Fig. 5(a) has A–A, A–B, B–A, and B–B combinations. When the interaction is connected by an inversion center, A–B and B–A are the same. In the case

TABLE 5
Overlap Integrals S($\times 10^{-3}$) in $2\cdot ClO_4$ and $4\cdot ClO_4$

$2\cdot ClO_4$	A···A	A···B B···A	B···B
I ($-x$, $-y$, $-z$)	−8.22	−18.05	4.81
II ($-x$, $-y$, $1-z$)	9.18	−3.38	−2.22
III ($2-x$, $1-y$, $1-z$)	2.53	0.26	0.00
IV ($-x-1$, $-y$, $1-z$)	−3.58	9.81 #0.50	0.91
$4\cdot ClO_2$			
I ($2-x$, $1-y$, $1-z$)	9.31	−22.70	−14.11
II ($x-1$, y, z)	−4.02	−1.97	−0.75
III ($2-x$, $1-y$, $1-z$)	3.43	−11.05	−5.62
IV ($x-1$, y, $z-1$)	1.66	0.78 #10.88	−4.10
V ($1-x$, $1-y$, $1-z$)	0.05	−0.40	2.48

of $2\cdot ClO_4$, the energy difference between HOMO and the next HOMO is large (0.13 eV), indicating that the intramolecular charge separation is significant (nearly A^0B^+) in accordance with the difference of the bond distances. Therefore, the B part in the TMT-bi-TTF molecule constructs a dimerized half-filled band, resulting in the relatively poor conductivity of the Mott insulating state.

In contrast to $2\cdot ClO_4$, the cation radical salt $4\cdot ClO_4$ has a fairly high conductivity (6.9 S/cm) with small activation energy (35 meV). The C(3)–C(4) and C(11)–C(12) bonds have the same distance (1.37(1) Å) as shown in Fig. 7(a), indicating a mixed-valence state. The cation radical salt forms a conducting sheet in the ac plane to make a segregated column. There are five intra- and interstack interactions between the cation radicals (Fig. 5(b) and Table 5). Interestingly, the two overlaps (I and II) are made up of the whole molecules, i.e., Figs. 7(a) and (b), whereas the other two (III and IV) are constructed by the interaction between only one TTF moiety of the cation radical, i.e., Figs. 7(c) and (d). The interstack interaction V is weak and may be neglected in the following discussion. The donor packing in $4\cdot ClO_4$ is also regarded as a β'-type dimerized structure. Although this dimer structure resembles that of β'-(BEDT-TTF)$_2\cdot ICl_2$ (36), the interdimer interactions are strong enough to lead to a two-dimensional conducting sheet. In the molecular orbital calculations, the next HOMO has appeared very close to the HOMO level ($\Delta E = 0.08$ eV). The next HOMO and HOMO are mainly located on the left (A) and right (B) halves of the molecule, respectively (Fig. 7(a)), and have the correct symmetry of TTF HOMO. The A and B units within the same molecule have the interaction of the order of $1/2\Delta E = 0.04$ eV, i.e., 4×10^{-3} as the orbital overlap, but this is no longer intermolecular interactions. Therefore, each intermolecular interaction has four kinds of interactions (A–A, A–B, B–A, and B–B) like those in $2\cdot ClO_4$. From the crystal symmetry (*P*-1), one unit cell contains two donors. As shown in Fig. 5(b), two donor molecules, which are connected by the interaction I, form a dimer unit. The face-to-face distance in Fig. 7a is 3.40 Å, and the overlap integral of the conduction orbitals seems to be fairly large [I: (A–B) = (B–A) $= -22.7\times10^{-3}$]. Because these two molecules are connected by an inversion center, the A part is located above the B part of another molecule so that there is large A–B interaction. There are considerable interdimer interactions II and III, spreading in the ac plane; this makes a two-dimensional conducting sheet. Because one donor has two TTF parts, this conducting sheet has a double-sheet structure stacking along the *b*-axis. There are no short S···S contacts less than the sum of van der Waals radii (3.70 Å) in the side-by-side overlap in Fig. 7(b), but the six S···S contacts (3.70–3.83 Å) can contribute to make a conducting path [II: (A–B) = (B–A) $= -11.1\times10^{-3}$]. The face-to-face interaction (III) and the side-by-side interaction (IV) seem to be strong through the S···S short contacts (III: 3.69 Å in Fig. 7(c); IV: 3.45, 3.46 and 3.59 Å in Fig. 7(d). Although the interactions III and IV are mediated by only one TTF part, these interactions are moderately large [III: (A–A) $= 4.0\times10^{-3}$; IV: (B–A) $= -10.9\times10^{-3}$]. Consequently, $4\cdot ClO_4$ shows fairly high

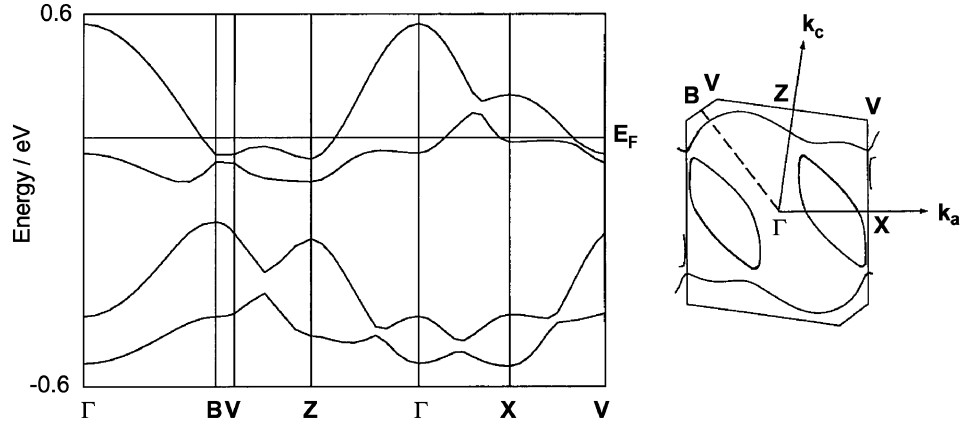

FIG. 8. Energy band structure and Fermi surface of $4\cdot ClO_4$.

conductivity with small activation energy, reflecting a two-dimensional band structure in contrast to the one-dimensional β'-phase.

Energy Band Structure

Energy band structure of $\mathbf{4} \cdot ClO_4$ calculated on the basis of the tight-binding approximation from these overlap integrals is depicted in Fig. 8. Since we treat each TTF part as an independent molecule, the energy band is effectively quarter-filled. One unit cell contains four TTF parts, so that there appear four energy levels, having two holes. This situation is the same as the usual 2:1 charge-transfer salts. The Fermi surface consists of closed parts, located between the Γ and X points, and open parts running along the *ka*-axis. In principle, these two parts are generated by two overlapping cylinders, one of which is located on the Γ point, and the other is centered on the X point, and each of which has a cross-section of approximately 50% of the first Brillouine zone, though that on the Γ point is larger than that on the X point. These two cylinders reflect the double sheet structure of the conducting sheet; one single sheet contains two quarter-filled TTF parts, resulting in the 50% cross-section. These two sheets have significant interaction, so that the Fermi surface is rearranged at which these cylinders cross each other, leading to the closed and the open parts. The resulting Fermi surface has a close resemblance to the usual κ-phase because the present compound is composed of a two-dimensional network of units strongly dimerized by interaction I. This is also obvious from the energy bands, where the upper two levels are separated from the lower two by the dimerization gap. Owing to this dimerization, each hole, located on each dimer, is in the Mott insulating state, in agreement with the moderately high but activated conducting behavior of the present compound.

ACKNOWLEDGMENTS

Financial support for this study was provided by Grant-in-Aid for Scientific Research on Priority Areas from Ministry of Education, Science and Culture, Japan (06243105) and by CREST of JST (Japan Science and Technology Corporation). We would like to thank Prof. Haruo Matsuyama, Muroran Institute of Technology, for helpful discussions.

REFERENCES

1. F. Wudl, G. M. Smith, E. J. Hufnagel, *J. Chem. Soc., Chem. Commun.* 1453 (1970).
2. F. Wudl, D. Wobshall, and E. J. Hufnagel, *J. Am. Chem. Soc.* **94,** 670 (1972).
3. J. Ferraris, D. O. Cowan, V. Walatka Jr., and J. H. Rerlstein, *J. Am. Chem. Soc.* **95,** 948 (1973).
4. J. H. Perlstein, *Angew. Chem., Int. Ed. Engl.* **16,** 519 (1977).
5. J. M. Williams, J. R. Ferraro, R. J. Thorn, K. D. Carlson, U. Geiser, H. H. Wang, A. M. Kini, and M. H. Whangbo, "Organic Superconductors (Including Fullerenes)," Prentice-Hall, Engelwoods Cliffs, NJ, 1992.
6. M. R. Bryce and L. C. Murphy, *Nature* **309,** 119 (1984).
7. D. J. Sandman and G. P. Ceasar, *Isr. J. Chem.* **27,** 293 (1986).
8. T. Otsubo, Y. Aso, and K. Takimiya, *Adv. Mater.* **8,** 203 (1996).
9. M. R. Bryce, *J. Mater. Chem.* **5,** 1481 (1995).
10. M. Adam and K. Müllen, *Adv. Mater.* **6,** 439 (1994).
11. M. R. Bryce, *Chem. Soc. Rev.* **20,** 355 (1991).
12. K. Bechgaard, K. Lerstrup, M. Jørgensen, I. Johannsen, and J. Christensen. In The Physics and Chemistry of Organic Superconductors" (G. Saito and S. Kagoshima Eds), p. 349. Springer-Verlag, Berlin, 1990.
13. V. Y. Lee, R. R. Schumaker, E. M. Engler, and J. J. Mayerle, *Mol. Cryst. Liq. Cryst.* **86,** 317 (1982).
14. Y. N. Kreitsberga, A. S. Édzhinya, R. B. Kampare, and O. Y. Neiland, *J. Org. Chem. USSR* 1312 (1989).
15. M. Iyoda, Y. Kuwatani, M. Oda, Y. Kai, N. Kanehisa, and N. Kasai, *Angew. Chem., Int. Ed. Engl.* **29,** 1062 (1990), and references cited therein.
16. J. L. Segura and N. Martín, *Angew. Chem., Int. Ed. Engl.* **40,** 1372 (2001).
17. M. R. Bryce, *J. Mater. Chem.* **10,** 589 (2000).
18. M. B. Nielsen, C. Lomholt, and J. Becher, *Chem. Soc. Rev.* **29,** 153 (2000).
19. H. Tatemitsu, E. Nishikawa, Y. Sakata, and S. Misumi, *Synth. Metals* **19,** 565 (1987).
20. J. Y. Becker, J. Bernstein, A. Ellern, H. Gershtenman, and V. Khodorkovsky, *J. Mater. Chem.* **5,** 1557 (1995).
21. D. E. John, A. J. Moore, M. R. Bryce, A. S. Batsanov, and J. A. K. Howard, *Synthesis* 826 (1998).
22. D. E. John, A. J. Moore, M. R. Bryce, A. S. Batsanov, M. L. Leech, and J. A. K. Howard, *J. Mater. Chem.* **10,** 1273 (2000).
23. M. Iyoda, Y. Kuwatani, N. Ueno, and M. Oda, *J. Chem. Soc., Chem. Commun.* 153 (1992).
24. M. Iyoda, E. Ogura, K. Hara, Y. Kuwatani, H. Nishikawa, T. Sato, K. Kikuchi, I. Ikemoto, and T. Mori, *J. Mater. Chem.* **9,** 335 (1999).
25. M. Iyoda, Y. Kuwatani, K. Hara, E. Ogura, H. Suzuki, H. Ito, and T. Mori, *Chem. Lett.* 599 (1997)
26. U. Kux, H. Suzuki, S. Sasaki, and M. Iyoda, *Chem. Lett.*, 183 1995.
27. M. Iyoda, Y. Kuwatani, E. Ogura, K. Hara, H. Suzuki, T. Takano, K. Takeda, J. Takano, K. Ugawa, M. Yoshida, H. Matsuyama, H. Nishikawa, I. Ikemoto, T. Kato, N. Yoneyama, J. Nishijo, A. Miyazaki, and T. Enoki, *Heterocycles* **54,** 833 (2001).
28. T. Mori, A. Kobayashi, Y. Sasaki, H. Kobayashi, G. Saito, and H. Inokuchi, *Bull. Chem. Soc. Jpn.* **57,** 627 (1984).
29. D. L. Green, *J. Org. Chem.* **44,** 1476 (1979).
30. M. Iyoda, M. Hasegawa, J. Takano, K. Hara, and Y. Kuwatani, *Chem. Lett.* 590 (2002).
31. M. Iyoda, M. Hasegawa, Y. Kuwatani, H. Nishikawa, K. Fukui, S. Nagase, and G. Yamamoto, *Chem. Lett.* 1146 (2001).
32. K. Lahlil, A. Moradpour, C. Bowlas, F. Menou, P. Cassoux, J. Bonvoisin, J.-P. Launay, G. Dive, and D. Dehareng, *J. Am. Chem. Soc.* **117,** 9995 (1995).
33. H. Spanggaard, J. Prehn, M. B. Nielsen, E. Levillain, M. Allain, and J. Becher, *J. Am. Chem. Soc.* **122,** 9486 (2000).
34. M. Iyoda, K. Hara, Y. Kuwatani, and S. Nagase, *Org. Lett.* **2,** 2217 (2000).
35. S. Nagase, to be published.
36. T. Mori, H. Inokuchi, *Solid State Commun.* **62,** 525 (1987).